Inorganic Chemistry

Article

pubs.acs.org/IC

Tuning Transverse Anisotropy in Co^{III}–Co^{II}–Co^{III} Mixed-Valence Complex toward Slow Magnetic Relaxation

Dayu Wu,*[,†,‡] Xingxing Zhang,[‡] Ping Huang,[‡] Wei Huang,[†,‡] Mingyue Ruan,[§] and Z. W. Ouyang*[,§]

[†]School of Petrochemical Engineering, Changzhou University, Changzhou, Jiangsu 213164, P. R. China

[‡]School of Chemistry and Chemical Engineering, Anqing Normal University, Anqing, Anhui 246011, P. R. China

[§]Wuhan National High Magnetic Field Center, Huazhong University of Science and Technology, Wuhan 430074, P. R. China

Supporting Information

ABSTRACT: Two cobalt mixed-valence complexes with different substituents have been prepared and structurally characterized by single-crystal X-ray diffraction to alter slow magnetic relaxation by tailoring the transverse anisotropy. The trinuclear complexes $[(L^1)_4Co_3(H_2O)_2](NO_3)_4\cdot CH_3OH\cdot 5H_2O$ (**1**-NO_3) and $[(L^2)_4Co_3(H_2O)_2](NO_3)_4\cdot 6H_2O$ (**2**-NO_3) feature a distorted octahedral Co(II) strongly hindered in a trinuclear Co^{III}–Co^{II}–Co^{III} mixed-valence array. Detailed magnetic studies of **1**-NO_3 and **2**-NO_3 have been conducted using direct- and alternating-current magnetic susceptibility data. In accordance with variable-field magnetic susceptibility data at low temperatures, high-field electron paramagnetic resonance (HF-EPR) spectroscopy reveals the presence of an easy-plane anisotropy ($D > 0$) with a significant transverse component, E, in complexes **1**-NO_3 and **2**-NO_3. These findings indicate that the onset of the variation of distortion within complex **2**-NO_3 leads to a suppression of quantum tunneling of the magnetization within the easy plane, resulting in magnetic bistability and slow relaxation behavior. Consequently, the anisotropy energy scale associated with the relaxation barrier, 5.46 cm^{-1} ($\tau_o = 1.03 \times 10^{-5}$ s), is determined by the transverse E term. The results demonstrate that slow magnetic relaxation can be switched through optimization of the transverse anisotropy associated with magnetic ions that possess easy-plane anisotropy.

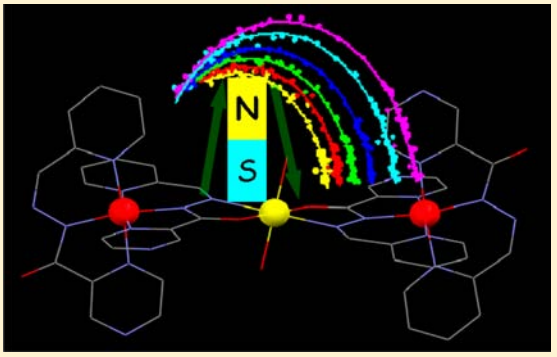

INTRODUCTION

Single-molecule magnets (SMMs) constitute a major scientific target because of their potential applications in high-density magnetic memories and quantum-computing devices.[1,2] For the majority of known SMMs containing transition metal aggregates, the energy barrier [$\Delta U = |D|S^2$ for integral and $\Delta U = |D|(S^2 - {}^1/_4)$ for half-integral spin] for magnetization reversal is enhanced via the combination of a large spin S of the ground state and a significant negative zero-field splitting parameter D under the spin Hamiltonian model described by $\hat{H} = D\hat{S}_z^2 + E(\hat{S}_x^2 - \hat{S}_y^2) + g\mu_B\hat{S}H$.[3−6] However, recently, the molecular anisotropy (D) in magnitude proved to be possible compared to controlling over the large total spin (S_T).[7,8] The new discovery of mononuclear complexes rather than polynuclear aggregates has renewed our understanding of the factors governing slow magnetic relaxation associated with global anisotropy. Typically, single-center lanthanide and actinide complexes have been widely shown to exhibit slow magnetic relaxation.[9−14] Mononuclear first-row transition metal complexes with slow magnetic relaxation were relatively rare because fast quantum tunneling magnetization (QTM) through the mixing of ±Ms levels may prevent the slow magnetic relaxation through a thermally activated mechanism.[15−23] Recently, Chang, Long, and co-workers mainly concentrated on species with low coordination numbers, i.e., high-spin trigonal-pyramidal Fe(II) species[18,19] and tetrahedral Co(II) mononuclear single-molecule magnets.[15,16] Murugesu et al. reported a Co(II) mononuclear molecule with distorted square-pyramidal geometry, and consequently, slow magnetic relaxation was observed.[17] Just recently, Cano and co-workers reported the first example of a severely distorted octahedral Co(II) complex with positive axial magnetic anisotropy ($D > 0$) that exhibits field-induced slow magnetic relaxation behavior.[22]

The type of complex is important not only because the relaxation mechanism is not typical for polynuclear SMMs but also because the relaxation process involving only the ground state or the participation of some excited states can be manipulated via the modulation of the ligand field. Although the slow relaxation of magnetization can be observable for a $D > 0$ system under the external field, magnetic anisotropy D, which depends on the spin−orbit coupling effect, is generally not easy to predict and/or control.[24] As an alternative property, the transverse anisotropy barrier (E) was identified as a possible source of slow magnetic relaxation behavior in the cobalt(II) complex, which prompted the search for obtaining the larger transverse anisotropy based on mononuclear Co^{2+} complexes with an $S = {}^3/_2$ ground state.[22,25] In this case, the energy barrier of magnetization reversal should be revised as $\Delta U = |E|(S^2 - {}^1/_4)$

Received: April 30, 2013
Published: September 17, 2013

for a half-integral spin, as described in the easy axis case. However, high-frequency electron paramagnetic resonance (HF-EPR) spectra as an efficient tool to simulate the accurate information regarding both axial and transverse magnetic anisotropy were not widely recorded when considering spin ground state anisotropy. The systematic modulation of the transverse anisotropy that consequently tunes the magnetic relaxation is still to be explored. Here, we report anion-specific formation of trinuclear cobalt complexes, $[(L^1)_4Co_3(H_2O)_2](NO_3)_4\cdot CH_3OH\cdot 5H_2O$ (abbreviated as **1**-NO_3 hereafter) and $[(L^2)_4Co_3(H_2O)_2](NO_3)_4\cdot 6H_2O$ (abbreviated as **2**-NO_3 hereafter), containing a deprotonated multidentate ligand as depicted in Scheme 1. The central cobalt ion is high-spin (Co^{II}, $t_{2g}^5e_g^2$) and sterically hindered by two peripheral diamagnetic (Co^{III}, $t_{2g}^6e_g^0$) subunits; hence, they can be considered as Co^{2+} mononuclear complexes from a magnetic point of view. With the aid of HF-EPR, this work aims to find whether such magnetically isolated complexes, where the Co^{2+} ion possesses a positive axial anisotropy ($D > 0$), can exhibit slow relaxation of magnetization. By tuning of the transverse anisotropy (E) through the subtle modification of the coordination sphere of the central high-spin Co(II), the slow magnetic relaxation toward the expected SMM property was obtained for complex **2**-NO_3.

Scheme 1. HL^1 and HL^2 Ligands Used in This Work

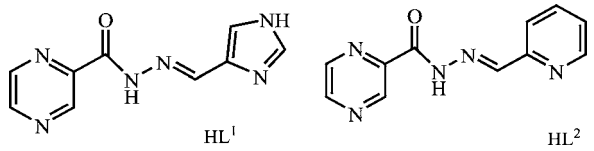

EXPERIMENTAL DETAILS

General. Unless otherwise noted, materials were obtained from commercial suppliers and were used without further purification. The infrared (IR) spectra were recorded (400−4000 cm^{-1} region) on a Nicolet Impact 410 Fourier transform infrared spectrometer using KBr pellets. Elemental analyses (C, H, and N) were conducted with a Perkin-Elmer 2400 analyzer. The magnetic susceptibility measurements were taken between 1.8 and 300 K for dc-applied fields ranging from 0 to 7 T. Direct-current (dc) susceptibility measurements were taken on a freshly filtered crystal sample of **1**-NO_3 and **2**-NO_3 wrapped in a polyethylene membrane. Complexes **1**-NO_3 and **2**-NO_3 were prepared rapidly to avoid any loss of solvent. Alternating-current (ac) susceptibility measurements were taken using an oscillating ac field of 3 Oe and ac frequencies ranging from 1 to 1500 Hz under 0 and 1000 Oe applied static fields, respectively. The high-field EPR data at 4.2 K were collected at Wuhan National High Magnetic Field Center (Huazhong University of Science and Technology) by a transmission-type spectrometer with operating frequencies of 77−350 GHz.

Synthesis. Pyrazine carbohydrozone was prepared according to the revised literature method.[26] Schiff base ligands HL^1 were synthesized by the condensation of pyrazine carbohydrozone and 4-imidazocarboxylate in a 1:1 ratio in methanol: IR (solid KBr pellet, HL^1) 3451.06(m), 1664.12(s), 1581.04(m), 1434.54(m), 1363.87(m), 1150.16(m), 782.95(m) and 674.32(m) cm^{-1}; ^1H NMR (DMSO-d_6) δ 9.12 (1H, s), 8.86 (1H, d), 8.43 (1H, d), 7.87 (1H, s), 7.43 (1H, s), 7.01 (1H, s). Anal. Calcd for $C_9H_8N_6O$: H, 3.73; C, 50.00; N, 38.87. Found: H, 3.68; C, 50.41; N, 38.68.

HL^2 was prepared in a similar manner except using pyridine-2-carboxylate for HL^2 instead of 4-imidazocarboxylate for HL^1: IR (solid KBr pellet, HL^2) 3450.68(m), 1662.46(s), 1580.24(m), 1431.23(m), 1360.16(m), 1151.63(m), 768.56(m), 704.08(m) and 668.02(m) cm^{-1}; ^1H NMR (DMSO-d_6) δ 9.14 (1H, s), 8.84 (1H, d), 8.78 (1H, d), 8.42 (1H, d), 7.98 (1H, d), 7.94 (1H, m), 7.58 (1H, m), 7.46 (1H, s). Anal. Calcd for $C_{11}H_9N_5O$: H, 3.99; C, 58.14; N, 30.82. Found: H, 4.12; C, 58.63; N, 30.75.

$[(L^1)_4Co_3(H_2O)_2](NO_3)_4\cdot CH_3OH\cdot 5H_2O$ (1-NO_3). Solid $Co(NO_3)_2\cdot 6H_2O$ (0.1 mmol, 29.0 mg) and ligand HL^1 (0.1 mmol, 21.6 mg) were combined in 25 mL of a CH_3OH/CH_3CN mixture [1:1 (v:v)], which afforded a dark-red solution that was magnetically stirred at room temperature for 20 min to obtain a clear solution, which was allowed to stand at room temperature. Dark-red block crystals suitable for X-ray diffraction were obtained after several days in the dark (9.2 mg, 25.1% based on ligand): IR (solid KBr pellet) 854.1(w), 1017.4(w), 1112.6(w), 1154.7(w), 1303.6(m), 1374.8(s), 1466.2(w), 1606.8(w) cm^{-1}. Anal. Calcd for $C_{37}H_{46}Co_3N_{28}O_{25}$: H, 3.17; C, 30.44; N, 26.87. Found: H, 3.19; C, 32.43; N, 28.65.

$[(L^2)_4Co_3(H_2O)_2](NO_3)_4\cdot 6H_2O$ (2-NO_3). Complex **2**-NO_3 was prepared in a manner similar to that used for **1**-NO_3 except using ligand HL^2 instead of HL^1 (11.9 mg, 32.5% based on ligand): IR (solid KBr pellet) 853.6(w), 1018.2(w), 1111.6(w), 1165.1(w), 1321.5(m), 1368.2(s), 1472.4(w), 1621.4(w), 1687.2(w) cm^{-1}. Anal. Calcd for $C_{44}H_{48}Co_3N_{24}O_{24}$: H, 3.28; C, 35.86; N, 22.81. Found: H, 3.23; C, 36.05; N, 22.49.

X-ray Crystallography. The crystal data for all the complexes have been collected on a Bruker SMART CCD diffractometer (Mo Kα radiation, λ = 0.71073 Å).[27] SMART was used for collecting frames of data, indexing reflections, and determining lattice parameters, SAINT for integration of the intensity of reflections and scaling, SADABS for absorption correction, and SHELXTL for space group and structure determination and least-squares refinement on F^2.[28] All structures were determined by direct methods using SHELXS-97 and refined by full-matrix least-squares methods against F^2 with SHELXL-97.[29] Hydrogen atoms were fixed at calculated positions, and their positions were refined by a riding model. All non-hydrogen atoms were refined with anisotropic displacement parameters. For complexes **1**-NO_3 and **2**-NO_3, the disordered nitrate group has been fixed by using isor, d_{fix}, and flat commands. Crystal data and cell parameters for **1**-NO_3 and **2**-NO_3 are listed in Table 1.

Table 1. Details of the Data Collection and Refinement Parameters of 1-NO_3 and 2-NO_3

	1-NO_3	2-NO_3
formula	$C_{37}H_{46}Co_3N_{28}O_{25}$	$C_{44}H_{48}Co_3N_{24}O_{24}$
crystal system	monoclinic	triclinic
space group	$P2_1/c$	$P\bar{1}$
a (Å)	22.285(12)	8.9739(4)
b (Å)	8.856(5)	10.1458(4)
c (Å)	28.583(16)	16.9041(5)
α (deg)		85.650(3)
β (deg)	100.228(7)	84.829(3)
γ (deg)		75.965(4)
V (Å^3)	5551(5)	1484.73(10)
Z	4	2
T (K)	293(2)	293(2)
goodness of fit	1.054	1.043
$R_1{}^a$ [$I > 2\theta(I)$]	0.0591	0.0745
$wR_2{}^b$ [$I > 2\theta(I)$]	0.1610	0.2130

$^aR_1 = \sum(|F_o| - |F_c|)/\sum|F_o|$. $^bwR_2 = \sum[w(F_o^2 - F_c^2)]/[\sum w(F_o^2)]^{1/2}$.

Structure Analysis. Trinuclear cobalt complex **1**-NO_3, $[(L^1)_4Co_3(H_2O)_2](NO_3)_4\cdot CH_3OH\cdot 5H_2O$, was obtained by reaction of HL^1 with $Co(NO_3)_2\cdot 6H_2O$ (1:1 molar ratio). Its crystal structure consists of cationic trinuclear $[(L^1)_4Co_3(H_2O)_2]^{4+}$ units as shown in Figure 1, together with additional anions. C−N bond distances of 1.362(3), 1.254(3), 1.344(2), and 1.345(2) Å for C(5)−N(3), C(14)−N(9), C(23)−N(15), and C(32)−N(21) bonds, respectively, together with the number of anions found in the lattice suggest that the protons on all the carbohydrozone groups get lost and HL^1 or HL^2 acts as a monoanionic ligand in the complex (denoted as L^1 or L^2, respectively).

dx.doi.org/10.1021/ic401057f | Inorg. Chem. 2013, 52, 10976−10982

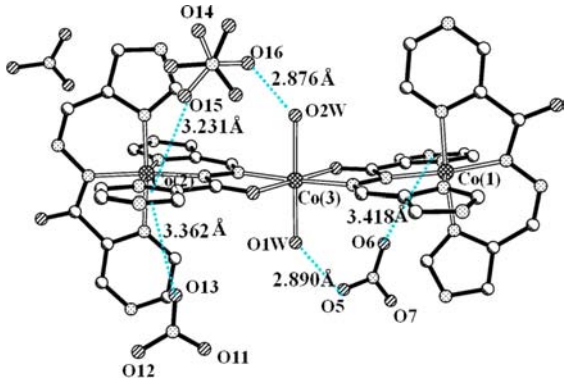

Figure 1. Stick model structure of compound **1**-NO_3 emphasizing the supramolecular association involving hydrogen bonding and anion−π contact with a D···A contact distance.

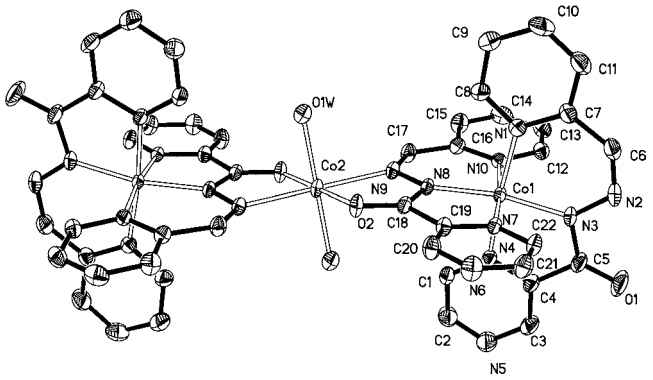

Figure 2. Crystal structure of compound **2**-NO_3 in the ellipsoid model. Hydrogen atoms, the uncoordinated solvent molecules, and anions have been omitted for the sake of clarity.

Two terminal cobalt atoms, Co(1) and Co(2), maintain the CoN_6 octahedral environment with the Co−N bond distance varying from 1.908(4) to 1.957(4) Å, while the central cobalt atom, Co(3), is six-coordinated by two sets of NO bidentate units from two different ligands in addition to two apical water molecules. The bond distances around the Co(3) center are obviously longer than those of Co(1) and Co(2); four Co−O and Co−N bond distances defining the equatorial plane vary between 2.082(3) and 2.106(4) Å. The axial position is occupied by *trans*-Co−O(hydrate) bonds of 2.082(3) and 2.134(2) Å, all of which are indicative of high-spin Co^{II} ion. As expected, low-spin Co^{3+} allows the ligand donor atoms to be significantly shorter (∼0.2 Å) than the analogous distances involving the high-spin Co^{2+} ion.[30] The oxidation state of three cobalt ions was assigned on the basis of these bond length considerations, charge balance, and BVS calculations. BVS values of 3.46, 3.45, and 2.04 for the Co(1), Co(2), and Co(3) centers, respectively, support the valence assignment on the basis of bond lengths.[31−33] Moreover, all the meridional bond angles involving the equatorial (N or O) and axial O atom are very close to 90° for the central Co(II), indicating a slight deviation from an ideal octahedron. The resulting Co(1)−Co(3)−Co(2) array is close to linearity with a Co(1)−Co(3)−Co(2) angle of ∼173°. Hence, the analysis of X-ray diffraction data is indicative of a mixed-valence trinuclear complex of the Co^{III}−Co^{II}−Co^{III} form, and the high-spin Co^{II} center is strongly hindered by two terminal metal coordination subunits as ligands.

Interestingly, the anionic units, i.e., NO_3^-, are linked to coordination water molecules in the form of O(1)W−H(1)WB···O(5) and O(2)W−H(2)WB···O(16) species with O···O separations of 2.890 and 2.876 Å, respectively, indicating strong hydrogen bonding interactions. Furthermore, O(6) and O(15) of the nitrate moieties in **1**-NO_3 complexes are oriented toward the π-face of pyrazine rings (Figure 1). Distances between oxygen atoms and the centroid of the pyrazine rings are 3.418(2) and 3.231(2) Å, respectively, indicative of the significant anion−π interaction.[34] Alternatively, the type of interaction is also evidenced by the shortest O···C separations for O(6) and O(15) in complex **1**-NO_3 of ∼2.95 and ∼3.05 Å, respectively, which are shorter than the sum of van der Waals radii of O and C (∼3.22 Å).[35]

Complex **2**-NO_3 was prepared under conditions similar to those of complex **1**-NO_3, except using $\mathbf{HL^2}$ instead of $\mathbf{HL^1}$. X-ray diffraction analysis revealed that complex **2**-NO_3 consists of cationic trinuclear $[(\mathbf{L^1})_4Co_3(H_2O)_2]^{4+}$ units with center symmetry as shown in Figure 2. Two terminal cobalt atoms, Co(1) and Co(1a) (symmetry code $a = -1 - x, -1 - y, -1 - z$), maintain the CoN_6 octahedral environment as found in complex **1**-NO_3 and are characteristic of Co^{III} ion judging from the short Co−N distance (1.921−1.967 Å). The bond distances around the Co(2) center are obviously longer than those of Co(1) ion; however, the distortion of high-spin Co(II) is different in the case of **2**-NO_3. The Co−O(aqua) axial bonding distance is obviously compressed to 2.052 Å compared to the equatorial plane consisting of an ∼2.144 Å Co−N(hydrazine) bond and a 2.091 Å Co−O(L) bond. Moreover, the O−Co−O bond angles involving equatorial and apical O atoms are 85.81° and 94.19°, respectively, reflecting the greater distortion compared to that of **1**-NO_3. As Co(2) occupies an inversion center, the resulting Co(III)−Co(II)−Co(III) array is linear by symmetry operation. The shortest intermolecular Co^{II}···Co^{II} distance is 8.856(2) Å for **1**-NO_3 and 8.974(2) Å for **2**-NO_3, which indicated the Co^{II} center is magnetically isolated and the trinuclear mixed-valence complex can be treated as the Co^{2+} mononuclear complex from the point of view of magnetism. The intrinsic magnetic anisotropy for the Co^{II} ion itself with a deformed sphere suggested the likelihood of slow magnetic relaxation.

The main structural difference is reflected in the local Jahn−Teller deformation of the central cobalt(II) ion between **1**-NO_3 and **2**-NO_3 (Table 2). In the case of **1**-NO_3, it is slightly distorted in the central

Table 2. Electronic and Structural Parameters of Complexes 1-NO_3 and 2-NO_3

	1-NO_3	**2**-NO_3
D (cm^{-1})	18.6	31.9
E (cm^{-1})	−1.7	−3.0
g_x	2.51	2.78
g_y	1.98	1.98
g_z	1.85	2.00
bond distance (Å)[a]	4.216	4.100
	4.166	4.180
	4.203	4.288
distortion type	slight elongation	compression

[a]Addition of the two bond distances along the three axes of the octahedron for the central Co(II): Co−O(aqua) + Co−O(aqua), Co−O(L) + Co−O(L), and Co−N(L) + Co−N(L) in sequence.

Co(II) and a slight elongation along the O(aqua)−Co−O(aqua) direction is observed as described above. However, the observation of a compression in the octahedron in **2**-NO_3 is unexpected.[36] The observed compression along the O(aqua)−Co-O(aqua) axis in **2**-NO_3 is due to the fact that the Co−O bonds are shortened compared to those in similar complex **1**-NO_3 (Table 2). To explain the difference between the two cobalt complexes, **1**-NO_3 and **2**-NO_3, our hypothesis is based on the more significant electron-deficient character of $\mathbf{HL^1}$ involving both pyrazine and imidazole groups compared to the $\mathbf{HL^2}$ ligand, favoring the formation of the interplay between anion−π contact and intramolecular hydrogen bonding in complex **1**-NO_3. As shown in Figure 1, the short nitrate···O(1W) and nitrate···O(2W) hydrogen bonds induce longer Co(3)−O(1W) and Co(3)−O(2W) bonds in a cooperative manner. However, because of the absence of obvious hydrogen bonding between nitrate and coordinated water in complex **2**-NO_3 as revealed by the crystallographic analysis, the Co−O(aqua) bond is greatly shortened and compression of the octahedral sphere for Co(II) is observed. Finally, it should be noted that the bonding distance in the equatorial plane also showed a significant difference in complex **2**-NO_3, the Co−N(L) distance being longer than the Co−O(L) distance by ∼0.1 Å,

dx.doi.org/10.1021/ic401057f | *Inorg. Chem.* 2013, 52, 10976−10982

which could potentially influence the transverse anisotropy within the $x-y$ plane.[37] Thus, this series is perfectly adapted to allow us to understand the effect of small structural modifications around the high-spin Co(II) ion on the electronic properties of the complexes (Table 2).

Magnetic Analysis. The dc SQUID data for crystal sample of **1**-NO_3 and **2**-NO_3 showed a slightly temperature dependent value of $\chi_M T$ (ca. 2.70 $cm^3\ mol^{-1}\ K$) over the temperature range 110−300 K (Figure 3), where χ_M is the molar magnetic susceptibility per $Co^{III}_2Co^{II}$ unit,

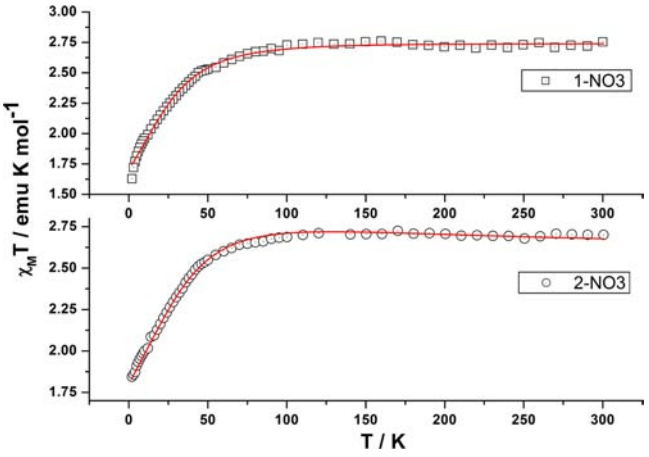

Figure 3. Temperature dependence of $\chi_M T$ for compounds **1**-NO_3 and **2**-NO_3 under a 2500 Oe magnetic field. Red solid lines represent the best fits with the Hamiltonian of eq 1.

falling within the range expected for only one high-spin d^7 Co^{II} ion (S = 3/2) in the range of 2.1−3.4 $cm^3\ mol^{-1}\ K$ for experimentally observed highly anisotropic Co^{II} ion.[38] When the temperature is further lowered, the $\chi_M T$ decreases more pronounced to reach values of 1.62 and 1.82 $cm^3\ mol^{-1}\ K$ for **1**-NO_3 and **2**-NO_3, respectively, at 2 K. The data can be fitted according to an $S = 3/2$ spin state with dominant zero-field splitting effects and Zeeman interactions under the action of the spin Hamiltonian.[39]

$$\hat{H} = D[\hat{S}_z^{\,2} - \frac{1}{3}S(S+1)] + g_{\parallel}\beta H_z S_z + g_{\perp}\beta(H_x S_x + H_y S_y) \quad (1)$$

where $D\hat{S}_z^{\,2}$ represents the splitting into two Kramers doublets in the absence of a magnetic field. The expressions of the magnetic susceptibility in eqs 1a−1c were easily derived from the Hamiltonian mentioned above, where N is Avogadro's number, μ_B is the Bohr Magneton, k_B is Boltzmann's constant, g is the Lande g value, and D is the zero-field splitting.

$$\chi_{\parallel} = \frac{N g_{\parallel}^{\,2} \mu_B^{\,2}}{k_B T} \times \frac{1 + 9e^{-2D/k_B T}}{4(1 + e^{-2D/k_B T})} \quad (1a)$$

$$\chi_{\perp} = \frac{N g_{\perp}^{\,2} \mu_B^{\,2}}{k_B T} \times \frac{4 + (3k_B T/D)(1 - e^{-2D/k_B T})}{4(1 + e^{-2D/k_B T})} \quad (1b)$$

$$\chi = \frac{\chi_{\parallel} + 2\chi_{\perp}}{3} \quad (1c)$$

Least-squares fitting of the experimental data through this expression (eqs 1a−1c) leads to $g_{\parallel} = 2.27(7)$, $g_{\perp} = 2.47(8)$, and $D = 35.1(3)$ for **1**-NO_3 and $g_{\parallel} = 1.69(2)$, $g_{\perp} = 2.61(5)$, and $D = 48.9(4)\ cm^{-1}$ for **2**-NO_3. It should be noted that the fitting quality is good even at very low temperatures without the inclusion of intermolecular magnetic interactions. The D value is comparable with those of other cobalt(II) complexes with axial-distorted square-pyramidal symmetry.[40] It should be noted that, as the variations of χT are in general not very sensitive to the sign of D, it is difficult to determine the absolute value of the axial ZFS parameter D only from magnetic susceptibility data derived from measurements on polycrystalline samples. However, a more sensitive probe in determining D values is HF-EPR measurement and the magnetization at intermediate fields and appropriate low temperatures (M vs H/T).

To further determine the magnitude and sign of the anisotropy parameter, we determined the field dependence of the magnetization of complexes **1**-NO_3 and **2**-NO_3 at fields ranging from 0 to 7 T between 2 and 10 K (Figure 4). The low-temperature experimental magnetization

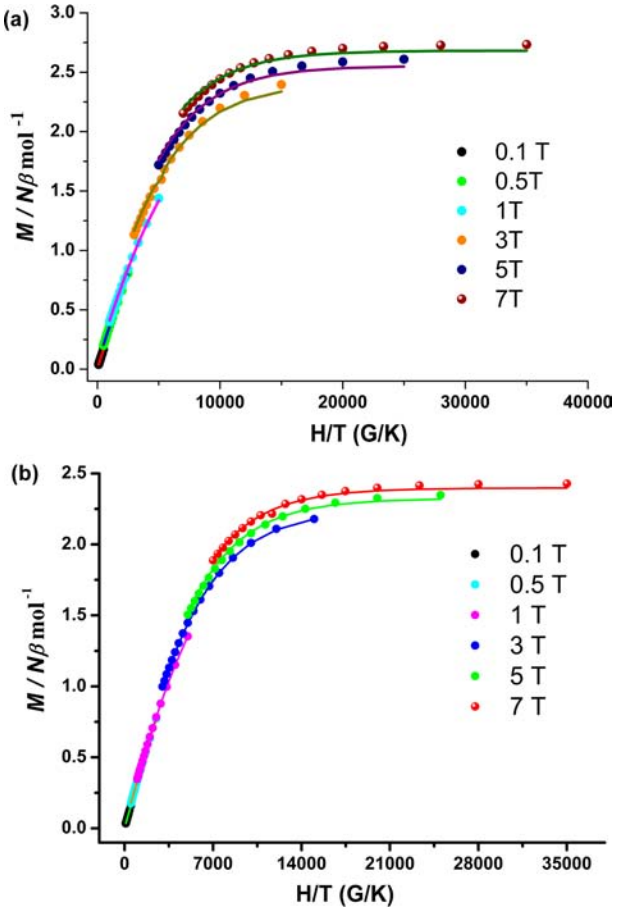

Figure 4. Low-temperature magnetization data for **1**-NO_3 (a) and **2**-NO_3 (b) collected in the temperature range of 2−10 K under various applied dc fields of 0.1−7 T. Solid lines correspond to best fits obtained with ANISOFIT verison 2.0 (see the text).

data were then analyzed using ANISOFIT version 2.0[41] adopting the spin Hamiltonian given in the Introduction, which takes into account the axial (D) and transverse (E) magnetic anisotropies.

In this notation, positive D values stabilize the $\pm^1/_2$ ground state and negative D values stabilize the $\pm^3/_2$ ground state. The best-fit values of the parameters were as follows: $D = 20.8(7)\ cm^{-1}$, $E \leq 0.1\ cm^{-1}$, and $g = 2.3(9)$ with $f = 0.025$ for **1**-NO_3 and $D = 29.8(8)\ cm^{-1}$, $E \leq 0.65\ cm^{-1}$, and $g = 2.4(3)$ with $f = 0.01$ (solid lines in Figure 4) for **2**-NO_3. Optimization by setting the initial D to a negative value does not converge to a reliable fit, indicating the correct choice of the positive sign. It should be noted while the D value is comparable to that observed by EPR spectroscopy, the E value is lower by at least 1 order of magnitude.

Although the magnetization data alone cannot conclusively establish the sign of D and any value of E obtained from magnetization data fits is tentative at best, high-field, high-frequency electron paramagnetic resonance (HF-EPR) spectra at low temperatures were recorded for the powder samples of complexes **1**-NO_3 and **2**-NO_3 to obtain definitive information about the zero-field splitting parameters (see Figures S5 and S6 of the Supporting Information). The low-temperature powder data are typical for an anisotropic system described by the zero-field

dx.doi.org/10.1021/ic401057f | Inorg. Chem. 2013, 52, 10976−10982

Hamiltonian $H = D\hat{S}_z^2 + E(\hat{S}_x^2 - \hat{S}_y^2) + g\mu_B\hat{S}H$. Here, three components are observed for both complexes **1**-NO_3 and **2**-NO_3 (Figure 5),

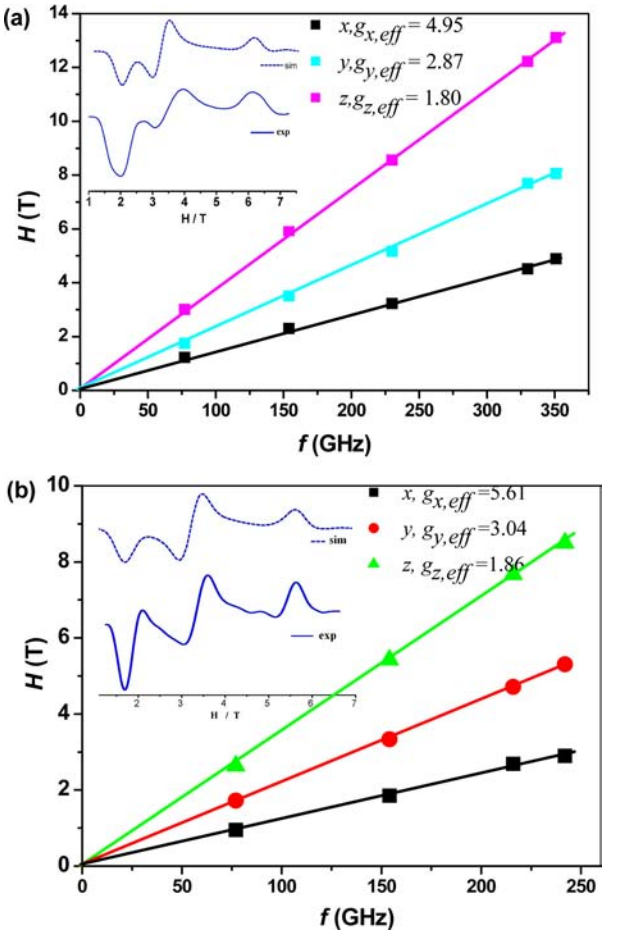

Figure 5. Frequency dependence of the high-frequency EPR peak positions deduced from studies of a powder sample of **1**-NO_3 (a) and **2**-NO_3 (b) at 4.2 K in Figures S5 and S6 of the Supporting Information. The inset is the best simulation (···) and experimental spectra (—) of 154 GHz in derivative mode at 4.2 K (see the text).

corresponding to transitions between two Kramers doublets ($m_s = \pm^1/_2$, and $m_s = \pm^3/_2$) according to the selection rule $\Delta m_s = \pm 1$, with one high-field component [effective Landé constant $g_{z,\text{eff}} = 1.80(3)$ for **1**-NO_3 and 1.86(4) for **2**-NO_3] separated from two low-field components [$g_{x,\text{eff}} = 4.95(2)$ and $g_{y,\text{eff}} = 2.87(7)$ for **1**-NO_3, and $g_{x,\text{eff}} = 5.61(3)$ and $g_{y,\text{eff}} = 3.04(4)$ for **2**-NO_3]. This pattern of g values is characteristic of an orbitally nondegenerate ground state with a positive D value,[42] which is reminiscent of the other high-spin Co(II) complex with a positive ZFS.[16,22] The g values of **2**-NO_3 were much larger than those of **1**-NO_3 in the $x-y$ plane. It is also worth noting that more obvious splitting between the two low-field components ($g_{x,\text{eff}}$ and $g_{y,\text{eff}}$) in the spectra of **2**-NO_3, i.e., $\Delta H = 1.56$ T at 154 GHz, versus that of **1**-NO_3 ($\Delta H = 0.97$ T at 154 GHz) is indicative of a more significant contribution from the small but non-negligible transverse E term.[43] Consequently, the difference in the perpendicular Landé constant for complex **2**-NO_3 ($\Delta g = 2.57$) is much larger than that of **1**-NO_3 ($\Delta g = 2.08$).

To precisely determine the uniaxial D and transverse E terms, spectral simulations were performed under the Hamiltonian given in the Introduction when considering spin ground state anisotropy. Assuming uniaxial anisotropy D is approximately 20−30 cm^{-1} as evaluated from M versus H/T analysis, a good simulation of the spectra can be achieved using Easyspin shown as the inset of Figure 5 by setting the anisotropic **g** tensor.[44] The parameters are as follows: $g_x = 2.51 \pm 0.01$, $g_y = 1.98 \pm 0.02$, $g_z = 1.85 \pm 0.02$, $D = 558.00 \pm 8.00$ GHz (18.6 ± 0.27 cm^{-1}), and $E = -51 \pm 3$ GHz (-1.7 ± 0.1 cm^{-1}) for **1**-NO_3 and $g_x = 2.78 \pm 0.01$, $g_y = 1.98 \pm 0.02$, $g_z = 2.00 \pm 0.01$, $D = 958.00 \pm 10.00$ GHz (31.9 ± 0.33 cm^{-1}), and $E = -91 \pm 3$ GHz (-3.0 ± 0.1 cm^{-1}) for **2**-NO_3. This is clear evidence that the D value is in agreement with the data obtained by fitting magnetization data and E is slightly different but significantly larger for **2**-NO_3 than for **1**-NO_3, which is evidenced by the difference in structure in the $x-y$ plane from the crystallographic analysis. We have also tried to remove the E parameter from the spin Hamiltonian; however, the simulation results are very poor, and no better results are obtained by allowing for an isotropic **g** tensor. It should also be noted that although the spin Hamiltonian formalism works properly to derive the **g** tensors and D and E in the theoretical calculation, more comprehensive calculation of magnetic data and HF-EPR spectra based on the orbitally dependent Hamiltonian is underway to better understand the correlation between the magnetic anisotropy and the structure of the complexes.[22,38,45,46]

The alternating-current (ac) magnetic susceptibilities of **1**-NO_3 and **2**-NO_3 were then investigated under zero and non-zero applied static fields, respectively (Figures S7−S10 of the Supporting Information). The ac measurement on crystalline sample **1**-NO_3 revealed the nearly zero out-of-phase ac susceptibility (χ_M'') under an applied field over the temperature range of 2.0−4.0 K. Both in-phase and out-of-phase signals exhibited negligible frequency dependence between 1 and 1500 Hz (Figure 6a and Figure S9 of the Supporting Information), indicating slow magnetic relaxation is difficult in **1**-NO_3 or the faster relaxation of magnetization is possible above 1500 Hz.

However, the ac data of complex **2**-NO_3 showed different results. A complete study of the ac susceptibility as a function of ac frequency was undertaken at different applied dc fields at 2.2 K, for example (Figure S10 of the Supporting Information). The optimal field for which the

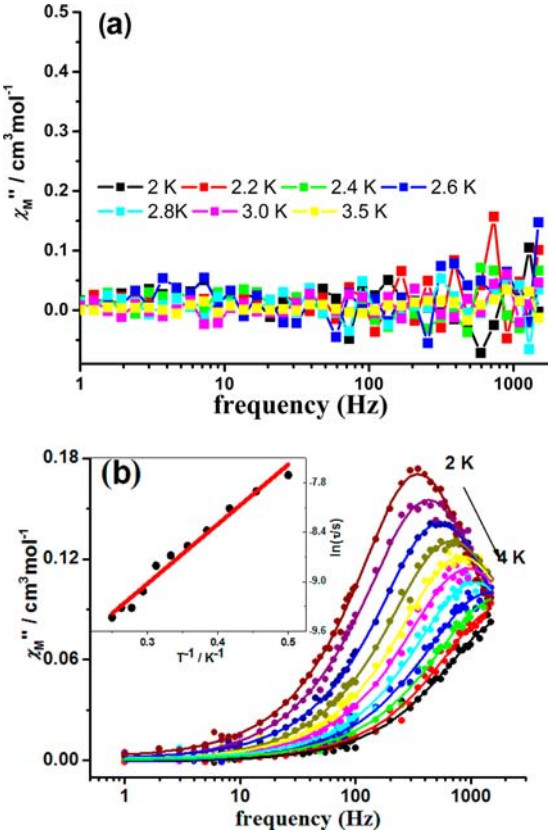

Figure 6. Variable-frequency out-of-phase ac susceptibility data for **1**-NO_3 (a) and **2**-NO_3 (b), collected under a 1000 Oe dc field over the temperature range of 2.0−4.0 K with a 3.0 G oscillating field. The inset of panel b shows the Arrhenius plot of **2**-NO_3 in the presence of 1000 Oe applied dc fields. The solid red line represents an Arrhenius fit to the data.

dx.doi.org/10.1021/ic401057f | Inorg. Chem. 2013, 52, 10976−10982

relaxation is the slowest was determined by plotting the relaxation time (τ) as a function of the applied field at a fixed temperature of 2.2 K (inset of Figure S10 of the Supporting Information). Although no peaks of χ_M'' are observed under zero dc magnetic field even at the highest frequency (ν = 1500 Hz), non-zero χ_M'' signals appeared when a small static dc field was applied, indicating a slowly relaxing magnetic moment. Moreover, under an applied field of 1.0 kG (this field was chosen because it induces slower relaxation), strong frequency-dependent maxima in both χ_M' and χ_M'' occurred below 10 K in the plot of temperature dependence ac data (Figure S8 of the Supporting Information). To obtain quantitative information regarding the spin relaxation barrier of **2**-NO_3, the frequency dependence of χ_M'' and χ_M' at the different temperatures was examined as shown in Figure 6b and a Debye model was used to extract relaxation times (τ) at different temperatures.[47,48] The results were employed in constructing the Arrhenius plots [$\tau = \tau_0 \exp(E_a/k_BT)$] shown as inset of Figure 6b. Assuming a thermally activated mechanism, a fit to the linear data would provide the activation energy (E_a = 5.6 cm^{-1}) and the pre-exponential factor ($\tau_0 = 1.03 \times 10^{-5}$ s). The τ_o value observed for **2**-NO_3 is at the higher boundary of the experimental range found for SMMs and is at least 5 orders of magnitude slower than expected for other Co^{2+} single-molecule magnets.[49] The large τ_o in magnitude is common for a Co^{2+} mononuclear single-molecule magnet and caused by the fact that the direct one-phonon process (Van-Vleck contribution), two-phonon Orbach process, and Raman process all contribute to the thermally activated mechanism, which along with quantum tunneling is responsible for the magnetization relaxation in SMMs.[22]

The Cole−Cole plots for **2**-NO_3 at different temperatures under a 1.0 kG dc field also display signatures of slow magnetic relaxation (Figure 7).[50] Fitting the data using the generalized Debye model as the following

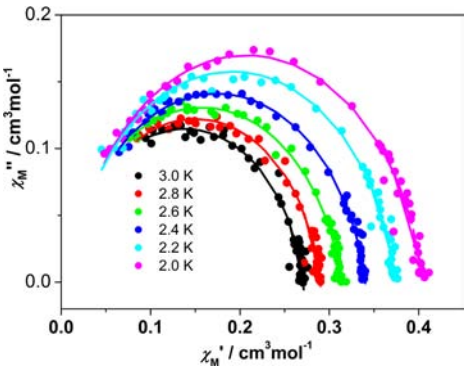

Figure 7. Cole−Cole plot of χ_M'' vs χ_M' over the temperature range of 2.0−3.0 K under a 1000 Oe applied dc field for compound **2**-NO_3. The solid line represents a least-squares fitting of the data to a distribution of single-relaxation processes.

expression (eq 2) gives the calculated values of α with the relatively narrow range between 0.07 and 0.12 at the different temperatures (Table S2 of the Supporting Information), which is indicative of a relatively narrow distribution of relaxation times.[51,52]

$$\chi''(\chi') = -\frac{\chi_0 - \chi_S}{2\tan(1-\alpha)\frac{\pi}{2}} + \sqrt{(\chi' - \chi_S)(\chi_0 - \chi') + \frac{(\chi_0 - \chi_S)^2}{4\tan^2(1-\alpha)\frac{\pi}{2}}} \quad (2)$$

Although complex **1**-NO_3 presented similar dc magnetic susceptibility data together with zero-field splitting (D), no slow relaxation of magnetization is observed for complex **1**-NO_3 even under a 1000 Oe field. However, the higher-frequency (>1500 Hz) data should be obtained to check whether the fast relaxation occurs with the lower barrier energy. This somewhat unexpected result can be generally attributed to the existence of fast quantum tunneling of the magnetization (QTM) through the thermal relaxation barrier. However, for a noninteger spin system with easy-plane anisotropy, such as **1**-NO_3 and **2**-NO_3, the role of E anisotropy in the case of the easy plane is not to promote the quantum tunneling but to create the barrier for magnetization reversal. Generally, a magnetic moment is difficult to direct along a preferred axis for a quantum spin subjected to easy-plane anisotropy ($D > 0$) due to the QTM effect.[53,54] However, the situation is quite different in the case of the magnetic moment associated with a macroscopic easy-plane system, and the appreciable transverse anisotropy would create a preferred axis, x or y (depending on the sign of E), within the x−y plane.[55] In such cases, the barrier height corresponding to rotation within the easy plane (x−y) would be dictated by $E(S^2 - {}^1/_4)$. Because $E \leq D/3$, a transverse barrier would normally be smaller than an axial one. Here, the energy of the transverse barrier for rotation in the x−y plane, given by an $E(S^2 - {}^1/_4)$ value of 6.0 cm^{-1} for **2**-NO_3, from the EPR experimental value is very close to the experimental barrier. This fact supports the idea that that the relaxation barrier is stemming from E and the transverse anisotropy energy barrier could be responsible for the slow magnetic relaxation behavior of **2**-NO_3. The lack of slow relaxation of magnetization for **1**-NO_3 within the available frequency of SQUID is due to the relatively small transverse barrier that makes the relaxation process so fast that it has moved completely out of the ac time scale.[56]

In conclusion, we present herein a new example of field-induced slow magnetic relaxation for a six-coordinate mononuclear Co(II) complex with positive anisotropy, despite the few other examples of four- or five-coordinated cobalt(II) complexes.[15−17] The absence of slow relaxation of magnetization in complex **1**-NO_3 is most likely due to fast quantum tunneling magnetization (QTM) through the mixing of $|\pm{}^3/_2\rangle$ levels that prevent the observation of slow magnetic relaxation through a thermally activated mechanism. Through tailoring of the transverse anisotropy of the center Co(II) in the trinuclear congener, **2**-NO_3, the relaxation dynamic is slowed and a frequency-dependent out-of-phase signal can be observed.[57] Ongoing work focuses on the preparation and characterization of more complexes through the introduction of the different ligand fields with the aim of enlarging the transverse anisotropy and obtaining the higher energy barrier. Toward this end, the comprehensive fabrication of the relaxation pathway is crucial to slowing the relaxation dynamics within single-molecule magnets to facilitate their potential applications.

■ ASSOCIATED CONTENT

Ⓢ Supporting Information

Crystallographic data (cif files) for **1**-NO_3 and **2**-NO_3, experimental procedures, and additional magnetic data. This material is available free of charge via the Internet at http://pubs.acs.org.

■ AUTHOR INFORMATION

Corresponding Authors

*E-mail: wudy@cczu.edu.cn.

*E-mail: zwouyang@mail.hust.edu.cn.

Notes

The authors declare no competing financial interest.

■ ACKNOWLEDGMENTS

This work was supported by NSFC (21001008, 21001007, and 21371010), and a portion of the magnetic measurements was supported by the State Key Laboratory of Physical Chemistry of Solid Surfaces (Xiamen University, Xiamen, China). D.W. appreciates Prof. Jihu Su and Dr. Wei Tong from the University of Science and Technology of China for kindly discussing the HF-EPR data. We thank the anonymous reviewers for the positive comments concerning the quality of the manuscript, and some opinions were directly used in the final work.

REFERENCES

(1) Gatteschi, D.; Sessoli, R. *Angew. Chem., Int. Ed.* **2003**, *42*, 268.
(2) Sessoli, R.; Gatteschi, D.; Caneschi, A.; Novak, M. A. *Nature* **1993**, *365*, 141.
(3) Bogani, L.; Wernsdorfer, W. *Nat. Mater.* **2008**, *7*, 179.
(4) Aromí, G.; Brechin, E. K. *Struct. Bonding (Berlin, Ger.)* **2006**, *122*, 1.
(5) Bagai, R.; Christou, G. *Chem. Soc. Rev.* **2009**, *38*, 1011.
(6) Molecular Magnets Issue of *Dalton Transactions*; Brechin, E. K., Ed.; Royal Society of Chemistry: Cambridge, U.K., 2010.
(7) Milios, C. J.; Vinslava, A.; Wernsdorfer, W.; Moggach, S.; Parsons, S.; Perlepes, S. P.; Christou, G.; Brechin, E. K. *J. Am. Chem. Soc.* **2007**, *129*, 2754.
(8) Milios, C. J.; Piligkos, S.; Brechin, E. K. *Dalton Trans.* **2008**, 1809.
(9) Ishikawa, N.; Sugita, M.; Wernsdorfer, W. *J. Am. Chem. Soc.* **2005**, *127*, 3650.
(10) Jiang, S.-D.; Wang, B.-W.; Sun, H.-L.; Wang, Z.-M.; Gao, S. *J. Am. Chem. Soc.* **2011**, *133*, 4730.
(11) AlDamen, M. A.; Clemente-Juan, J. M.; Coronado, E.; Marti-Gastaldo, C.; Gaita-Arino, A. *J. Am. Chem. Soc.* **2008**, *130*, 8874.
(12) Rinehart, J. D.; Long, J. R. *J. Am. Chem. Sci.* **2009**, *131*, 12558.
(13) Jiang, S. D.; Wang, B. W.; Su, G.; Wang, Z. M.; Gao, S. *Angew. Chem., Int. Ed.* **2010**, *49*, 7448.
(14) Magnani, N.; Apostolidis, C.; Morgenstern, A.; Colineau, E.; Griveau, J.-C.; Bolvin, H.; Walter, O.; Caciuffo, R. *Angew. Chem.* **2011**, *50*, 1696.
(15) Zadrozny, J. M.; Long, J. R. *J. Am. Chem. Soc.* **2011**, *133*, 20732.
(16) Zadrozny, J. M.; Liu, J.; Piro, N. A.; Chang, C. J.; Hill, S.; Long, J. R. *Chem. Commun.* **2012**, *48*, 3927.
(17) Jurca, T.; Farghal, A.; Lin, P.-H.; Korobkov, I.; Murugesu, M.; Richeson, D. S. *J. Am. Chem. Soc.* **2011**, *133*, 15814.
(18) Freedman, D. E.; Harman, W. H.; Harris, T. D.; Long, G. J.; Chang, C. J.; Long, J. R. *J. Am. Chem. Soc.* **2010**, *132*, 1224.
(19) Harman, W. H.; Harris, T. D.; Freedman, D.; Fong, E. H.; Chang, A.; Rinehart, J. D.; Ozarowski, A.; Sougrati, M. T.; Grandjean, F.; Long, G. J.; Long, J. R. *J. Am. Chem. Soc.* **2010**, *132*, 18115.
(20) Weismann, D.; Sun, Y.; Lan, Y.; Wolmershäuser, G.; Powell, A. K.; Sitzmann, H. *Chem.—Eur. J.* **2011**, *17*, 4700.
(21) Lin, P.-H.; Smythe, C. N.; Gorelsky, J. S.; Maguire, S.; Henson, J. N.; Korobkov, I.; Scott, L. B.; Gordon, C. J.; Baker, T. R.; Murugesu, M. *J. Am. Chem. Soc.* **2011**, *133*, 15806.
(22) Vallejo, J.; Castro, I.; Ruiz-Garcıá, R.; Cano, J.; Julve, M.; Lloret, F.; Munno, G. D.; Wernsdorfer, W.; Pardo, E. *J. Am. Chem. Soc.* **2012**, *134*, 15704.
(23) Chandrasekhar, V.; Dey, A.; Mota, A. J.; Colacio, E. *Inorg. Chem.* **2013**, *52*, 4554.
(24) Gomez-Coca, S.; Cremades, E.; Aliaga-Alcalde, N.; Ruiz, E. *J. Am. Chem. Soc.* **2013**, *135*, 7010.
(25) Feng, X.; Liu, J.; Harris, T. D.; Hill, S.; Long, J. R. *J. Am. Chem. Soc.* **2012**, *134*, 7521.
(26) Wu, D. Y.; Xie, L. X.; Zhang, C. L.; Duan, C. Y.; Zhao, Y. G.; Guo, Z. J. *Dalton Trans.* **2006**, *29*, 3528.
(27) *SMART & SAINT Software Reference Manuals*, version 6.45; Bruker Analytical X-ray Systems, Inc.: Madison, WI, 2003.
(28) Sheldrick, G. M. *SADABS: Software for Empirical Absorption Correction*, version 2.05; University of Göttingen: Göttingen, Germany, 2002.
(29) Sheldrick, G. M. *SHELXL97: Program for Crystal Structure Refinement*; University of Göttingen: Göttingen, Germany, 1997.
(30) Abedin, T. S. M.; Thompson, L. K.; Miller, D. O. *Chem. Commun.* **2005**, 5512.
(31) Brese, N. E.; O'Keeffe, M. *Acta Crystallogr.* **1991**, *B47*, 192.
(32) Brown, I. D.; Altermatt, D. *Acta Crystallogr.* **1985**, *B41*, 244.
(33) O'Keeffe, M.; Brese, N. E. *J. Am. Chem. Soc.* **1991**, *113*, 3226.
(34) Frontera, A.; Gamez, P.; Mascal, M.; Mooibroek, T. J.; Reedijk, J. *Angew. Chem., Int. Ed.* **2011**, *50*, 9564.
(35) Bondi, A. *J. Phys. Chem.* **1964**, *68*, 441.
(36) Mantel, C.; Hassan, A. K.; Pecaut, J.; Deronzier, A.; Collomb, M.-N.; Duboc-Toia, C. *J. Am. Chem. Soc.* **2003**, *125*, 12337.
(37) Sato, O.; Cui, A. L.; Matsuda, R.; Tao, J.; Hayami, S. *Acc. Chem. Res.* **2007**, *40*, 361.
(38) (a) Boča, R. *Coord. Chem. Rev.* **2004**, *248*, 757 and references cited therein. (b) Titiš, J.; Boča, R. *Inorg. Chem.* **2011**, *50*, 11838.
(39) (a) Kahn, O. *Molecular Magnetism*; VCH: New York, 1993. (b) Miyasaka, H.; Clérac, R.; Campos-Fernández, C. S.; Dunbar, K. R. *Inorg. Chem.* **2001**, *40*, 1663.
(40) Lloret, F.; Julve, M.; Cano, J.; Ruiz-García, R.; Pardo, E. *Inorg. Chim. Acta* **2008**, *361*, 3432.
(41) Shores, M. P.; Sokol, J. J.; Long, J. R. *J. Am. Chem. Soc.* **2002**, *124*, 2279.
(42) Banci, L.; Bencini, A.; Benelli, C.; Gatteschi, D.; Zanchini, C. *Struct. Bonding (Berlin, Ger.)* **1982**, *52*, 37.
(43) Stoll, S.; Schweiger, A. *J. Magn. Reson.* **2006**, *178*, 42.
(44) Stoll, S.; Britt, R. D. *Phys. Chem. Chem. Phys.* **2009**, *11*, 6614.
(45) Lohr, L. L.; Miller, J. C.; Sharp, R. R. *J. Chem. Phys.* **1999**, *111*, 10148.
(46) Palii, A.; Tsukerblat, B.; Clemente-Juan, J. M.; Coronado, E. *Int. Rev. Phys. Chem.* **2010**, *29*, 135.
(47) Standley, K. J.; Vaughan, R. A. *Electron Spin Relaxation Phenomena in Solids*; Hilger: London, 1969.
(48) Rinehart, J. D.; Long, J. R. *Dalton Trans.* **2012**, *41*, 13572.
(49) Atherton, N. M. *Principles of Electron Spin Resonance*; Ellis Horwood Limited: Chichester, U.K., 1993.
(50) Cole, K. S.; Cole, R. H. *J. Chem. Phys.* **1941**, *9*, 341.
(51) Orbach, R. *Proc. R. Soc. London, Ser. A* **1961**, *264*, 458.
(52) Kramers, H. A. *Proc. K. Ned. Akad. Wet.* **1930**, *33*, 959.
(53) Caneschi, A.; Gatteschi, D.; Sessoli, R.; Barra, A. L.; Brunel, L. C.; Guillot, M. *J. Am. Chem. Soc.* **1991**, *113*, 5873.
(54) Barra, A. L.; Gatteschi, D.; Sessoli, R. *Phys. Rev. B* **1997**, *56*, 8192.
(55) Hill, S.; Edwards, R. S.; Aliaga-Alcalde, N.; Christou, G. *Science* **2003**, *302*, 1015.
(56) Gatteschi, D.; Sessoli, R.; Villain, J. *Molecular Nanomagnets*; Oxford University Press: Oxford, U.K., 2006.
(57) Carlin, R. L. *Magnetochemistry*; Springer-Verlag: New York, 1986.